Structure of the parameter space of a ring cavity

J. A. C. Gallas

Höchstleistungsrechenzentrum, Forschungszentrum Jülich, D-52425 Jülich, Germany
(Fax: +49-2461/61-2430)

Abstract. We describe the structure of the parameter space of a ring cavity according to a model due to Ikeda. We show how families of isoperiodic solutions in phase space organize themselves in parameter space: The parameter space of a ring cavity contains an infinite number of regularly arranged self-similar shrimp-shaped domains of stability. The regularities found for the ring cavity have the same generic arrangement observed for a canonical quartic map depending on two parameters. We explain the mathematical origin of the regularities and discuss a number of questions related to them in both discrete-time and continuous-time models, and suggest a possible way of cleaning chaos from some laser systems.

PACS: 42.50.Md; 05.45.+b

A result that solidified during the last few years as being a fundamental truth pervading all natural sciences is that even simple deterministic models can exhibit chaotic behaviors which are essentially indistinguishable from truly random processes. One immediate consequence of this is that the distinction between deterministic and stochastic effects becomes a rather delicate matter and their mathematical description not necessarily unique. Thus, it seems appropriate to reconsider well established subjects which rest upon specific mathematical formulations, either "stochastic" or "deterministic", seeking for a more unified description.

The ability of generic dynamical systems to display rather complicated behaviors has been known at least since last century when Poincaré described the existence of "homoclinic" phenomena while studying questions related to the stability of a well-known dynamical system in Celestial Mechanics: the solar system. Since then, there has been always a considerable interest in investigating and classifying all flavors of dynamical behaviors which are buried and delimited by the so-called *stable* and *unstable* manifolds, i.e., by the multidimensional surfaces implied by the equations of motion. This interest has experienced an explosive growth during the last 20 years or so.

A great difficulty in studying the plethora of dynamical behaviors living on the exceedingly complicated multidimensional surfaces generated by physical models is caused by the fact that *variables* and *parameters* appear always deeply intertwined in practice and in any theoretical description. The traditional way of separating and classifying possible dynamical states is by, first, representing in *phase-space* diagrams all possible behaviors and then, second, delimiting in *parameter-space* diagrams all regions characterized by similar properties of interest. While alone the delimitation of all possible behaviors in phase space is not necessarily a trivial task, complete diagrams in parameter space are frequently harder to obtain because each individual point on such diagrams is usually obtained studying a whole phase-space diagram which might contain more than one dynamical behavior, depending on initial conditions, for example.

This paper reports diagrams in parameter space classifying dynamical behaviors for a model proposed by Ikeda [1] to describe the dynamics of an externally driven ring cavity containing a Kerr medium. By now, laser systems of all kinds have been employed as powerful tools to probe nonlinear dynamics in general and to probe the intrinsic dynamics of lasers [2]. We hope that the detailed diagrams reported here might stimulate experiments to check the regularities predicted by the model of Ikeda as well as its limits of applicability. However, the regularities being presently reported were observed in several other dynamical systems being therefore generic.

We wish to investigate the organization of islands of periodic and aperiodic ("chaotic") behaviors in dynamical systems defined either by discrete-time or continuous-time models, searching for similarities. We start in Sect. 1 with the discrete-time model of Ikeda, showing that the parameter space of the ring cavity contains a very regular structure, composed of certain "shrimp-like" islands of periodicity which appear embedded inside wide "seas of chaos", with an arrangement essentially similar to that recently found to exist in different mathematical models [3]. Then, in Sect. 2, we present a model that contains a parameter space analogon

---

Dedicated to H. Walther on the occasion of his 60th birthday
Inspired by the proximity of the end of the year, it may become clear after glancing at the figures below that our motivation for selecting the model of Ikeda was mainly dictated by our wish to offer the "bunten Christbaum" in Fig. 1 together with the other color figures to Prof. Walther, as our birthday present to him

to the ring cavity but that has the great virtue of allowing *analytical* results to be easily obtained for it. Exploring certain algebraic varieties underlying this model, Sect. **3** shows that the whole organization found in parameter space is ruled by some very special numbers which satisfy an algebra of radicals implicit in (14) and (15) below. We also show how a result already known to Euler provides a powerful means of bypassing completely the necessity of studying the phase space, allowing one to concentrate directly on the structure and properties of the parameter space. In Sect. **4** we investigate regularities in parameter space of a dynamical system defined by a differential equation, the continuous-time model defined by (23), showing that there one finds regular islands of chaos embedded in seas of regularity. We then exploit the regularity with which chaos appears to describe a possible way of "cleaning" chaotic behaviors from laser systems. Finally, Sect. **5** summarizes our conclusions and offers some suggestions for further research.

1 Parameter space of the ring cavity

Under suitable conditions [1], the behavior of a ring cavity may be described by the equation

$$z_{t+1} = a + b z_t e^{i\theta(z_t)}, \tag{1}$$

known as the Ikeda map [4-8]. In this equation, the complex variable $z_t \equiv x_t + iy_t$ represents the electric field at the beginning of the t-th passage around the ring, a is related to the input amplitude and b is the coefficient of reflectivity of the partially reflecting output mirror. The quantity $\theta(z_t)$ is a relatively complicated functional of the amplitude inside the cavity. In the original formulation of Ikeda [1] one has

$$\theta(z_t) = |z_t|^2, \tag{2}$$

while Hammel et al. [5] considered

$$\theta(z_t) = \Delta - \frac{\delta}{1 + |z_t|^2}, \tag{3}$$

Δ being the empty-cavity detuning and δ an additional detuning when a nonlinear medium is present. Here we will consider the original model of Ikeda, (1) and (2). We observe that the parameter space of the Ikeda map with $\theta(z_t) = |z_t|^2$, (2), was previously considered by Carr and Eilbeck [7], while that with (3) was recently studied in [9] in connection with investigations of new phenomena due to the occurrence of degenerate tangencies between certain manifolds.

As is known [2], the transmitted field in the ring cavity is, in general, a multivalued function of the incident field. The transmitted field might be either a periodic or an aperiodic ("chaotic" or "turbulent") function [1, 4–8] depending on parameters and/or initial conditions.

Figure 1 shows several diagrams classifying parameter regions characterized by producing similar periodicities in the transmitted field. Each individual picture composing Fig. 1 was obtained as a color PostScript bitmap by discretizing the corresponding parameter intervals into a mesh of 600×600 equally spaced points and determining for each point the periodicity of the asymptotic solution (attractor) after a transient of 800 iterations. Iterations were performed along lines of constant reflectivity b, starting always at the

smallest input field-amplitude a from the arbitrary initial condition $z_0 \equiv 0.001 + i0.001$, discarding 800 iterations, determining and plotting periodicities subsequently. While determining periodicities along lines of constant b, the initial value $z = z_0$ was used only to start iterations at the smallest value of a, say a_{min} in each picture. To start iterations for each newly incremented value of a we "followed the attractor", i.e., used the last value of z_t obtained with the previous value of a as the initial condition for the newly incremented a.

All periods up to 24 were determined and are represented in Fig. 1 by the different colors. Absence of numerically detectable periodicities or periods longer than 24 were considered as "chaos" and plotted as white points in the diagrams. In this figure, green regions correspond to period-one (fixed points), dark-blue to period-two, light-blue to period three, red to period four, violet to period five, etc. One sees that adjacent to the wide green regions (period-one) one finds the characteristic period-two doublings, represented in dark-blue. Next, follow red regions indicating a new doubling (to period four) and so on. Adjacent to every island characterized by some period k one may recognize the first few members belonging to full cascades $k \times 2^n$, the "shrimps"[3], seen more clearly on the lower part of figure. As is the case with bifurcation diagrams, as the periodicity of the transmitted field increases, there is a rather strong reduction of the relative visible sizes of the parameter regions where families of solutions having identical periodicities are stable.

Increasing the maximum period plotted in the figures to 32 or 64 produced pictures virtually identical under the resolution of Fig.1. Notice that Fig. 1 is necessarily not complete since for a given set (a, b) of parameters, even though there might exist more than one stable solution for (1), it is only possible to plot *one* of them at a time. This difficulty is similar to the familiar one observed when plotting bifurcation diagrams [10] but, as is frequently the case, does not constitute any serious limitation.

Figure 1 displays a large number of regularities, the most prominent being perhaps the shape similarity of the regions corresponding to periodic motions and the regularity with which they appear distributed in parameter space. Dominant features are the shrimp-shaped clusterings of $k \times 2^n$ doubling cascades that were also seen in the parameter space of the Hénon map [3], their regular organization in parameter space and the strong compression of their visible "volume" as the periodicity increases.

An important question (discussed in the next section) is to understand the mathematical origin of all these regularities. Further, we would like to be able to predict where in parameter space one will find shrimps of stability for any arbitrary period k and to learn how to control the system so as to permit "jumping" directly and precisely, theoretically with a single move, from one region of stability to another, either with the same or with different period. In other words, *to find the proper group of transformations underlying the equation of motion that would allow one to move from one isoperiodic region to another, precisely.*
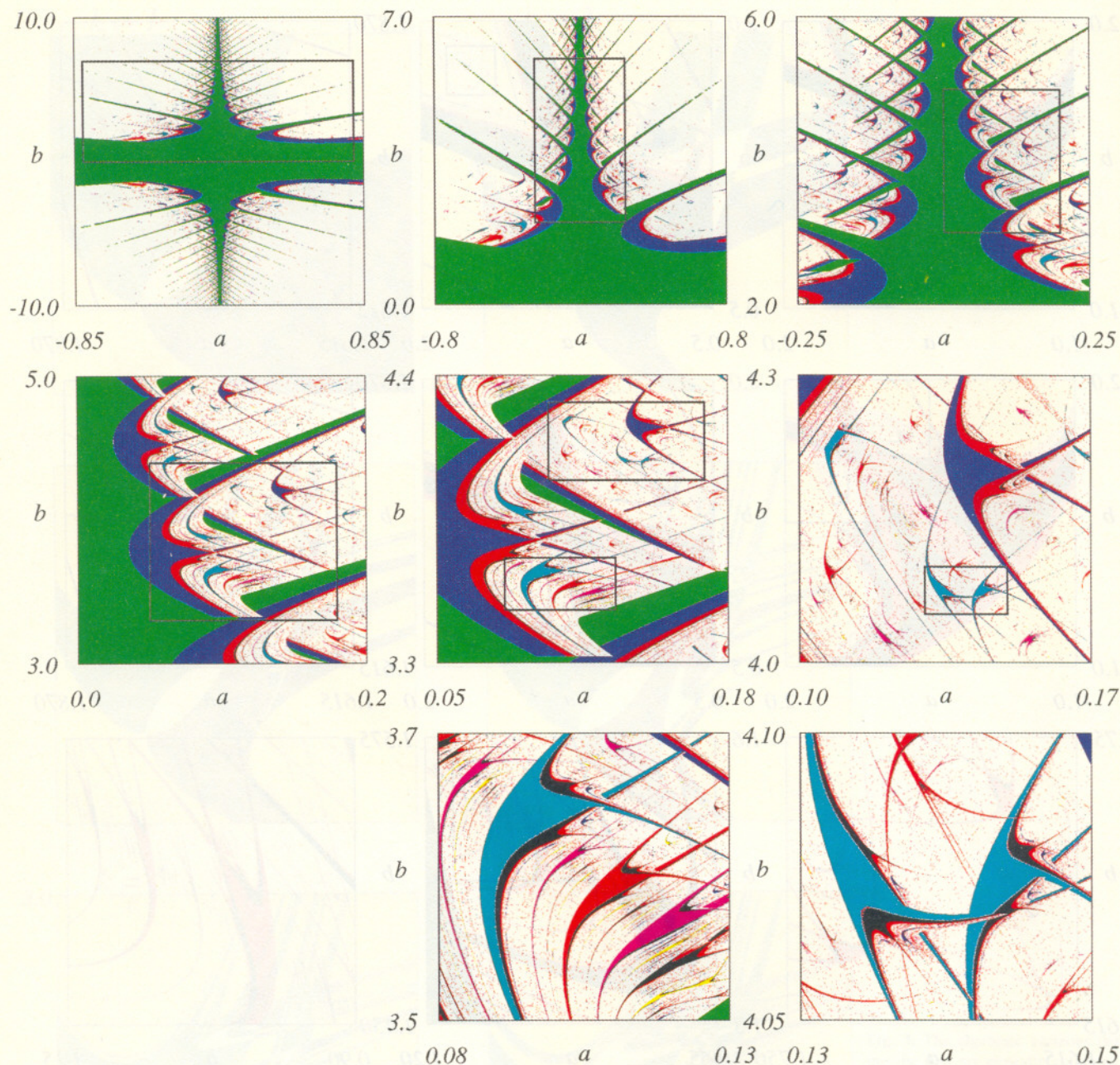
Fig. 1. Parameter space for the ring cavity, showing isoperiodic islands (*in colors*) embedded in a sea of chaos (*represented in white*). Green indicates period $k = 1$, dark-blue $k = 2$, light-blue $k = 3$, red $k = 4$, violet $k = 5$, etc. The two magnifications on the bottom show "shrimps": clusters characterized by a main periodicity k followed by an infinite sequence of adjacent bifurcations $k \times 2^n$. To enhance visibility in these figures, black was frequently used to represent regions of doublings $2k$ for high values of k

2 The origin of shrimps of stability

In this section, we describe analytically the mathematical origin of the regular shapes observed in the parameter space of the ring cavity as shown in Fig. 1. To this end, however, rather than working with (1) directly (which involves a complex variable and trigonometric functions), we simplify matters and consider a more convenient model that, while still retaining the dynamical features observed in the ring cavity, is considerably easier to deal with analytically. This model is defined [11] by the equation

$$x_{t+1} = f(x_t, a, b) = (a - x_t^2)^2 - b, \tag{4}$$

where x_t is a real variable and a and b are real and arbitrary parameters.

It is important to observe that this model by no means implies loss of generality. Quite to the contrary, since we may frequently assume generic equations of motion as being defined by expansions in Taylor series, the model defined in (4) contains the three terms of lowest order in x_t^2, i.e., nonlinearly in x_t and, therefore, represents the most fundamental model of nonlinear dynamics[12]. In some sense, the model of (4) represents a sort of a "hydrogen atom" of nonlinear
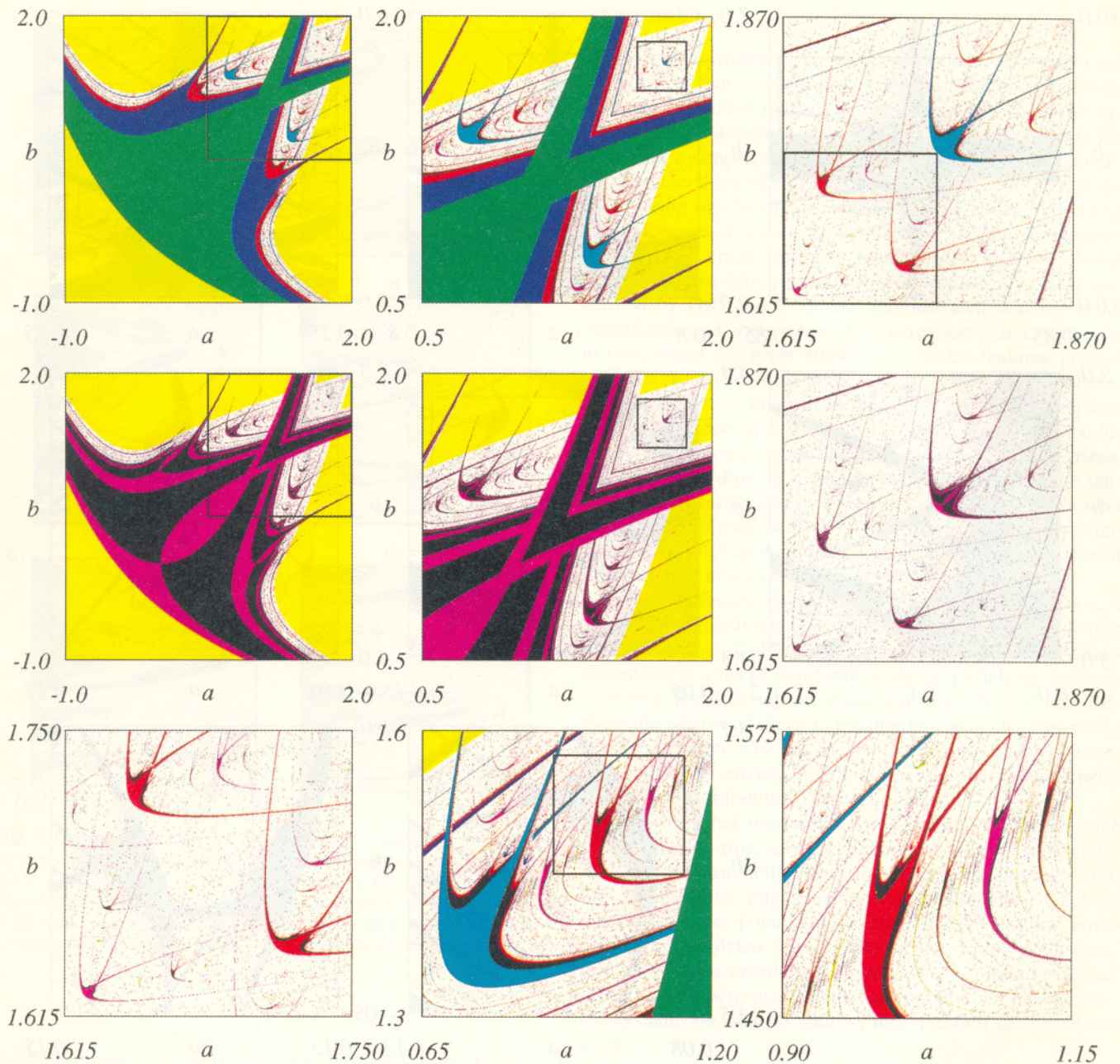
Fig. 2. Isoperiodic shrimps for the quartic map defined by (4). The middle row shows the parity of the multipliers m (see Sect. 3) for the canonical $k = 1$ shrimp (in green) shown with magnifications in the first row. Black indicates $m < 0$ and violet $m > 0$. The *last row* shows magnifications of portions of the parameter space containing shrimps similar to those found in the ring cavity (Fig. 1)

dynamics: it contains all ingredients of arbitrary models but is a convenient normal form allowing one to derive results analytically.

Figure 2 shows parameter-space diagrams for (4). On the row at the top one sees the "canonical" shrimp, i.e., that one starting with the lowest possible periodicity: 1×2^n. The single region of period $k = 1$ is represented in green, the two adjacent regions with period $k = 2$ are represented in dark-blue, the four regions with period 4 in red, etc. The row in the middle of the figure shows the *parity of multipliers* [11] for the same intervals of parameters as in the top row. The multiplier corresponding to a k-periodic orbit x_0,

$x_1, x_2, \cdots, x_k \equiv x_0$ is simply the derivative of $f_k(x, a, b)$, the k-th composition of the function $f(x_t, a, b)$ with itself. More explicitly:

$$m_k = f'_k(x, a, b) = \frac{df_k(x, a, b)}{dx}\bigg|_{x=x_0}$$
$$= f'(x_0)\, f'(x_1)\, \cdots\, f'(x_{k-1})\,, \quad (5)$$

giving, when applied to (4),

$$m_k = 4x_0(x_0^2 - a) \cdot 4x_1(x_1^2 - a) \cdots 4x_{k-1}(x_{k-1}^2 - a). \quad (6)$$

We say that the parity of m_k is positive when $m_k > 0$ and negative when $m_k < 0$. As one sees from Fig. 2, the
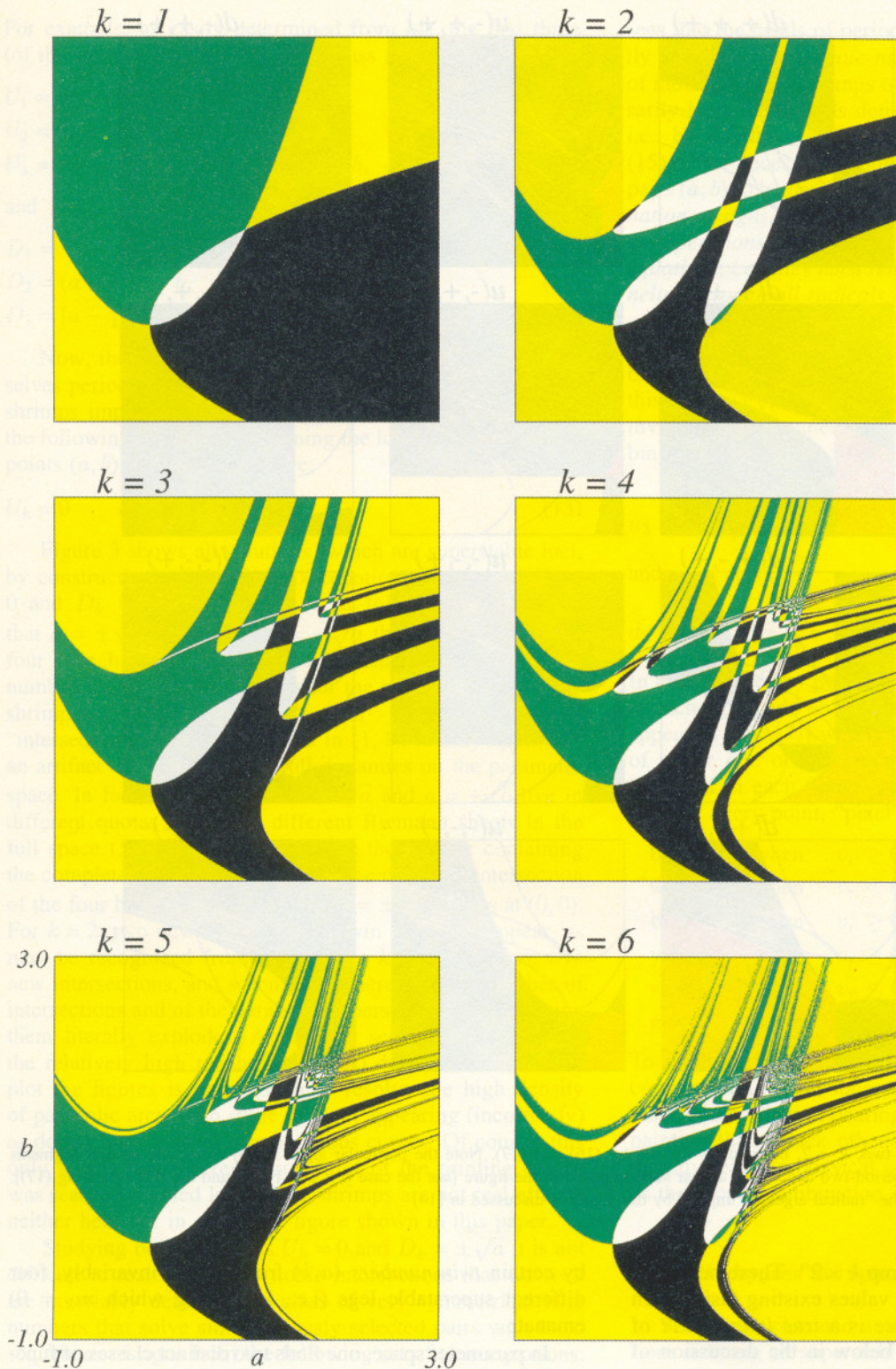
Fig. 3. The algebraic varieties defining the first six periodic solutions of (13), represented by the borders lines between regions of different colors. Colors codify the relative magnitudes of each k-periodic solution as follows: yellow: $u_k > 0$ and $d_k > 0$; black: $u_k > 0$ and $d_k < 0$; green: $u_k < 0$ and $d_k > 0$; white: $u_k < 0$ and $d_k < 0$. The scales shown apply to all six figures

multipliers expose the internal structure of each isoperiodic domain. Multipliers show that each individual *cell* of stability making the shrimp is divided into four quadrants, with adjacent quadrants having different parities. As is easy to recognize from (6), the lines delimiting regions of different parity correspond to lines characterized by $m_k = 0$. Such lines are known as "superstable" loci [13], loci which define

"centers" of stability inside each isoperiodic cell. From (4), one sees that all $m_k = 0$ loci in parameter space originate from trajectories passing in phase space through at least one of the zeros of the derivative of (4), namely, $x_t = 0$, $+\sqrt{a}$ or $-\sqrt{a}$. As one recognizes from the plots of the parity of the multipliers, the fundamental quantities ruling the regular organization of the parameter space are the "heads" of the
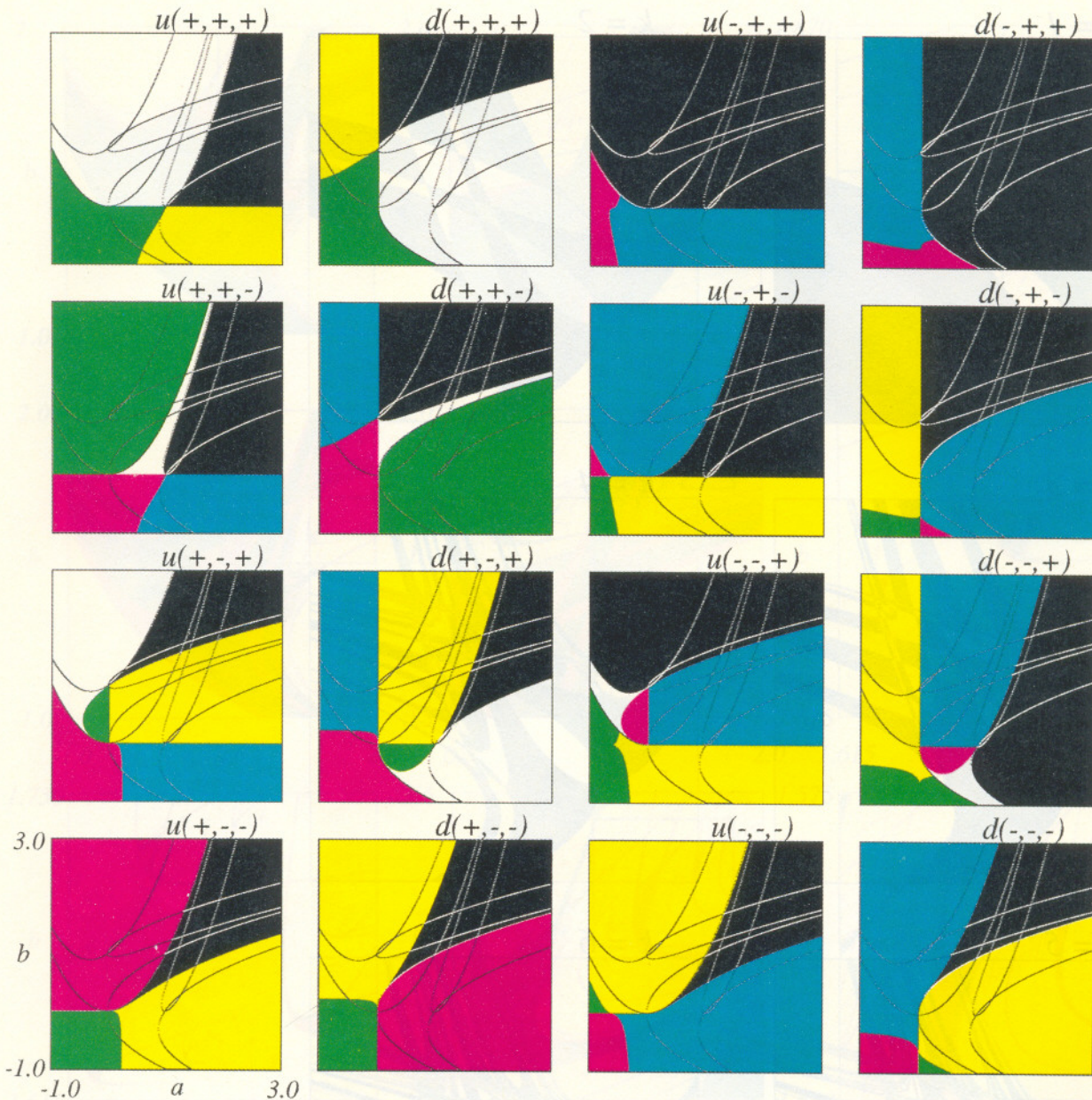
S208

Fig. 4. Boundaries of reality for period-two, $k = 2$, behavior as defined by (16) and (17). Note the particular signs which define the several segments composing the superstable structure of period-two and which appear superimposed in the figure [see the case $k = 2$ in Fig. 3 and the text following (17)]. The scales shown apply to all figures. The "radical algebra" implied by this figure is discussed in [14]

regions of period k of every shrimp $k \times 2^n$. These heads are defined by the unique parameter values existing inside each isoperiodic region for which there is a *true intersection* of both $m_k = 0$ loci, as explained below in the discussion of Fig. 3.

We already had the opportunity to discuss the organization of these regularities elsewhere [11]. Here, without going into too much technical details that will be provided elsewhere [14], we would like to summarize briefly a new result defined in (14) and (15) below: The *origin* of the beautiful mathematical mechanism that is at work in distributing privileges to very particular "noble" points in parameter space, points which are infinite in number and around which one invariably finds nucleation of stability. The key is provided

by certain *twin numbers* (a, b) from which, invariably, four different superstable legs (i.e., loci along which $m_k = 0$) emanate.

In parameter space, one finds two distinct classes of functions, more precisely distinct affine algebraic varieties, defining superstable loci:

(*i*) The *unique* class $U_k \equiv f_k(x_t = 0, a, b)$ determined by k−periodic orbits passing in phase space through the zero of the derivative at $x_t = 0$,

(*ii*) The *degenerate* class $D_k \equiv f_k(x_t = \pm\sqrt{a}, a, b)$ determined by k−periodic orbits passing in phase space through either one of the two remaining zeros of the derivative: $x_t = +\sqrt{a}$ or $x_t = -\sqrt{a}$.

For example, as easily determined from (4), the first three (of the infinite) members in each class are

$$U_1 = a^2 - b, \tag{7}$$
$$U_2 = [a - (a^2 - b)^2]^2 - b, \tag{8}$$
$$U_3 = \{a - [a - (a^2 - b)^2]^2 - b\}^2 - b, \tag{9}$$

and

$$D_1 = -b, \tag{10}$$
$$D_2 = (a - b^2)^2 - b, \tag{11}$$
$$D_3 = [a - \{(a - b^2)^2 - b\}^2]^2 - b. \tag{12}$$

Now, the fact that the zeros of the derivative are themselves periodic points living inside each cell composing the shrimps implies that for every $k = 1, 2, \ldots$ one must have the following equations containing the locations of the noble points (a, b) in parameter space:

$$U_k = 0 \quad \text{and} \quad D_k = \pm\sqrt{a}. \tag{13}$$

Figure 3 shows all solutions (which are superstable loci, by construction) of the first six equations implied by $U_k = 0$ and $D_k = \pm\sqrt{a}$. For $k = 1$, it follows from $U_1 = 0$ that $a = \pm\sqrt{b}$ and from $D_1 = \pm\sqrt{a}$ that $b = \pm\sqrt{a}$. These four branches are exactly those emanating from the twin number $(a, b) = (0, 0)$, the head of the canonical period-one shrimp plotted in green/dark-blue/red/$\cdots$ in Fig. 2. The other "intersection", the "tail" located in $(1, 1)$, is only *apparent*, an artifact of projecting the full dynamics on the parameter space. In fact, the branches $b = +\sqrt{a}$ and $a = +\sqrt{b}$ live in different quotas x, i.e., in different Riemann sheets in the full space (x, a, b), the space where the surface containing the complete dynamics is defined. The only real intersection of the four branches $a = \pm\sqrt{b}$ and $b = \pm\sqrt{a}$ occurs at $(0, 0)$. For $k = 2$, two new intersections (twin numbers) appear, as may be recognized from Fig. 3. For $k = 3$, there are five new intersections, and so on. As k increases, the number of intersections and of the parabolic superstable loci containing them literally explodes. As already seen for $k = 4$, even the relatively high resolution of 400 dots-per-inch used to plot the figures is not enough to resolve the high density of parabolic arcs, with some of them appearing (incorrectly) as dotted lines instead of continuous curves. Of course, this only means that the resolution limit of the printing device was reached. Dotted legs of the shrimps are not real effects, neither here nor in any other figure shown in this paper.

Studying both equations $U_k = 0$ and $D_k = \pm\sqrt{a}$ it is not difficult to realize that the noble intersections that we seek are invariably defined by a class of very symmetrical twin numbers that solve simultaneously selected pairs with fixed sequences of signs from the following set of twin equations:

$$a = \pm\sqrt{b \pm \sqrt{a \pm \sqrt{b \pm \sqrt{a \pm \cdots}}}}, \tag{14}$$

$$b = \pm\sqrt{a \pm \sqrt{b \pm \sqrt{a \pm \sqrt{b \pm \cdots}}}}, \tag{15}$$

where the number of radicals in each sequence is the same and is related in a simple manner to the periodicity k of each cell composing the shrimps. From (14) and (15), one clearly

sees that the heads of periodic shrimps are always necessarily defined by *algebraic numbers*, i.e., by *finite* sequences of radicals, while shrimps of aperiodic behavior must necessarily have their heads defined by *transcendental* numbers, i.e., by *infinite* sequences of radicals. Equations (14) and (15) define necessary conditions, "tunneling conditions", for pairs (a, b) to be heads of cells of stability: *for a fixed combination of signs, a and b must be simultaneously invariant to the operations indicated by the sequence of radicals in both equations, i.e., they must remain the same numbers after tunneling through all radicals.*

As an illustration of the algebra of radicals implied by (14) and (15), Fig. 4 shows the location of all superstable branches and heads of stability for period-two motions. In this case, we have to look for all pairs (a, b) which remain invariant while tunneling simultaneously through some combination of signs for all possible radicals defined as follows:

$$u_2 \equiv a \pm \sqrt{b \pm \sqrt{a \pm \sqrt{b}}} = 0 \tag{16}$$

and

$$d_2 \equiv b \pm \sqrt{a \pm \sqrt{b \pm \sqrt{a}}} = 0. \tag{17}$$

In Fig. 4, for every possible combination of signs [as defined in each figure and ordered in the same sequence as the signs appear in (16, 17)] we abbreviate by $v \equiv v_r + i v_i$ the value of either one of the complex numbers u_2 or d_2 (as also indicated in each figure) and use the following convention to paint every point, "pixel", in parameter space:

black	when	$v_r \geq 0$ and $v_i = 0$,
white	when	$v_r < 0$ and $v_i = 0$,
blue	when	$v_r \geq 0$ and $v_i > 0$,
yellow	when	$v_r \geq 0$ and $v_i < 0$,
violet	when	$v_r \leq 0$ and $v_i > 0$,
green	when	$v_r \leq 0$ and $v_i < 0$.

To facilitate the analysis, we added to Fig. 4 the skeleton corresponding to all superstable loci of period-two, painting them white when appearing against a black background or painting them black otherwise. From this figure, one may directly read the physical solutions to (16) and (17) as well as the proper combination of signs composing their parts.

3 How to bypass the space of variables

In Sect. 2 we obtained analytical expressions for the equations defining all superstable loci for (4) by considering two particular families of functions, U_k and D_k, which were generated by iterating the equation of motion in phase space from very special initial conditions, "critical points", defined by zeros of the derivative of the equation of motion. In this section, we show that, although such procedure is the standard one used today, at least in the case of polynomial equations of motion, it is possible to completely avoid having to work in phase space. This fact is not without interest since it not only allows one to greatly simplify and abbreviate the analysis but, much more importantly, allows one to

obtain analytical insight. By totally bypassing the space of variables we transform into an exercise in the theory of algebraic functions a subject that, after Poincaré and others, is currently dealt as a problem in topology. Since the number of dynamical systems with equations of motion that may be represented by polynomial series is not small, the procedure to be described here may be applied to a quite large number of physical situations with great advantage. Anyway, even though the method described in the next paragraph might be simple, the results that it generates are complicated and, at least, very different from what one is used to find in the literature.

As shown in Sect. 2, to locate the points of interest in parameter space, one has to deal with a set of two equations:

$$x = f_k(x, a, b), \qquad (18)$$
$$m_k = f'_k(x, a, b), \qquad (19)$$

where k represents the period of the solution [11]. The first equation defines the solution, while the second defines its multiplier, i.e., its stability [13]. To avoid having to consider the dynamics in phase space, all that needs to be done at the outset is to eliminate the variable x between both equations. For polynomial equations of motion this can be done following a procedure already known to Euler (1707–1783), namely, by calculating the *resultant* [15] between both polynomials.

For example, to determine the location and stability of period-one solutions (i.e., fixed points) for (4), from (18) and (19), one obtains the system

$$a^2 - b - x - 2ax^2 + x^4 = 0, \qquad (20)$$
$$-m - 4ax + x^3 = 0, \qquad (21)$$

where, for simplicity, we wrote $m \equiv m_1$. The resultant of these two equations is given by the determinant of a 7×7 matrix and leads to the following surface in the space (a, b, m):

$$m^4 - 12m^3 + (48 - 32ab)m^2 + 64(ab - 1)m$$
$$-256(a - b^2)(a^2 - b) = 0. \qquad (22)$$

In this way, without having to consider any sequence of iterates in the space of variables, one obtains an analytical expression for a surface defining, among other things, the boundaries of stability of period-one solutions. A particularly relevant portion of this surface is the slice of stability delimited by $-1 \leq m \leq 1$. For $m = 0$, the "center" of the interval of stability, one easily recognizes in the last term of (22) the relations defining the period-one loci of super-stability: $a = \pm\sqrt{b}$ and $b = \pm\sqrt{a}$, clearly reproducing the solutions of lowest order contained in the general expressions in (14) and (15) and plotted in Fig. 3. By studying solutions for $m = -1$ and for $m = 1$, one delimits the full interval of stability for period-one solutions. The period-two surface is defined by the determinant of a 31×31 matrix. In principle, analogous surfaces forming an infinite affine algebraic variety may be obtained for motions of any periodicity but we will not elaborate this any further here [14].

We conclude this section observing that, as is well-known, it is possible to encode and study dynamics using sequences of symbols, the so-called "symbolic dynamics".

The traditional approach in this field is to consider the dynamics in *phase-space*, codifying solutions with symbols like, L(eft), R(ight), etc. The sequences of signs in (14) and (15) open the possibility of an alternative characterization, an "algebra of radicals", based totally in *studying the dynamics directly in parameter space*, a procedure which expedites considerably the investigation of questions related to the stability of dynamical systems in general and allows one to relate the sequence of signs in (14) and (15) with the number and ordering of jumps between Riemann sheets [14]. As was shown in this Section, (14) and (15) are intrinsic properties of the dynamical systems, consequences of the dynamics, and might be derived without any knowledge or reference to what is going on in phase space.

4 How to clean chaos from driven systems

So far, we have considered only discrete-time dynamical systems and found that they are characterized by regular repetitions of isoperiodic shrimp-like regions embedded in seas of chaos. But, is it possible to have the opposite: similarly looking islands of chaos embedded in seas of regularity? And, if yes, is it possible to clean such islands of chaos from physical systems? The answer to both questions is affirmative as we now demonstrate. To this end, we will consider a continuous-time dynamical system, i.e., a system with its motion defined by differential equations, not discrete-time mappings.

Regular distributions of islands of chaos may be found in continuous-time models and seem to be relatively common features of such models. And, what is important from the point of view of practical applications, we find that *it is possible to clean chaos from wide regions in parameter space by driving the system properly with periodic forces having Fourier spectra more complicated than that of familiar trigonometric drives*. To see this, we consider what happens to, for example, a Duffing oscillator [16] when excited with the Jacobian elliptic function $\text{cn}(t, m)$, namely, to the equation

$$\ddot{x} + a\dot{x} + x^3 = b \cdot \text{cn}(t, m), \qquad (23)$$

where a, b and m are free parameters, m being now the standard notation for the parameter of elliptic functions [17] and having nothing to do with the multipliers of Sect. 3.

Figure 5 shows the wave form and the period of the function $\text{cn}(t, m)$ for some values of m. The parameter m provides a convenient way of moving continuously from the familiar trigonometric pumping, when $\text{cn}(t, m = 0) \equiv \cos(t)$, to a "hyperbolic pumping", when $\text{cn}(t, m = 1) \equiv \text{sech}(t)$. For m values in the range $0 < m < 1$, one has "intermediary" pumpings with rich and regular Fourier spectra [17]. From Fig. 5, one clearly sees that changes in m modify simultaneously both the wave form and the period of the oscillations.

As is known, one may use *Lyapunov exponents* [18] λ to produce a dichotomic division of the parameter space into regions where there are either chaotic behaviors, characterized by $\lambda > 0$, or periodic behaviors, characterized by $\lambda \leq 0$. The determination of Lyapunov exponents for differential equations is a quite computer-demanding task, and to obtain numerical values for exponents over a wide range of
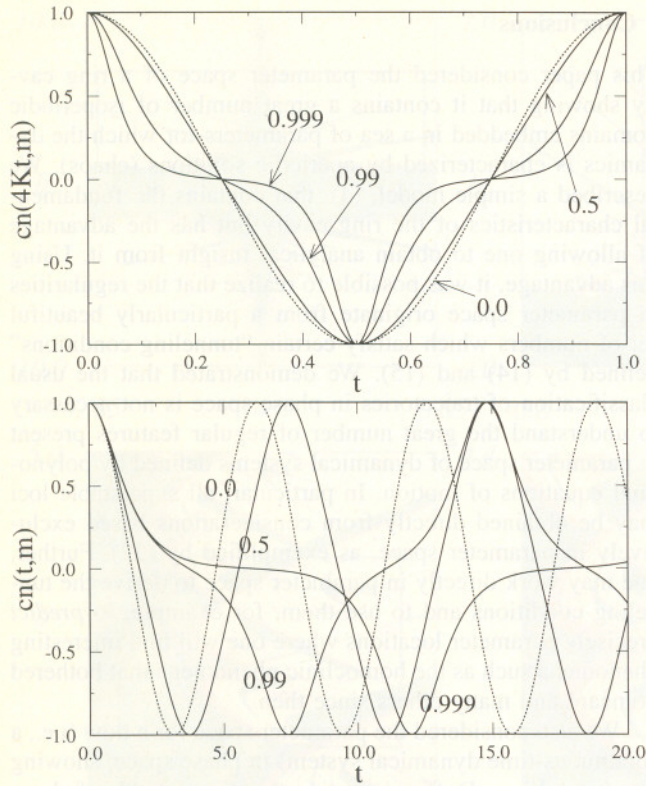
Fig. 5. Modifications of the wave form and periodicity of the elliptic function cn(t, m) for some values of m, as indicated by the numbers. *Dotted lines* correspond to cos(t). By varying m, one changes simultaneously the *wave form* and the *period* of the drive. The period of cn(t, m) is $4K(m)$ [17]

parameters, we used a fourth-order Runge-Kutta integrator to solve (23) together with up to 140 nodes in parallel, "farming", of an Intel Paragon XP/S 10, a scalable distributed multicomputer. Each of these nodes contains two i860 XP microprocessors (application processor, message processor), whose clock speed is 50 MHz, and 32 MB of memory. The theoretical peak performance of the i860 XP is 75 MFLOPS (64-bit arithmetic). In other words, sets of exponents were computed in parallel by an array of up to 140 workstations, each one computing exponents for a slice of the parameter space.

Figure 6 shows Lyapunov exponents obtained for $m = 0$, i.e., under the familiar trigonometric excitation, representing with black those parameters characterized by positive exponents (chaotic behaviors) and with white those characterized by non-positive exponents (periodic behaviors). From Fig.6 one easily recognizes the surprising existence of recurrent "islands" of chaotic behaviors embedded in "seas" of periodic behavior. As seen in Fig. 6, another interesting fact is that both the islands as well as their internal seas of periodic behaviors are very much similar to each other. In fact, all these islands of chaos seem to have a common underlying shape, the difference between islands being apparently only the "stretchings" that one needs to apply parallel to the a- and/or b- axis to make them congruent to each other. Therefore, *as the amplitude of the trigonometric pump increases, we observe a well-defined regular repetition of self-similar islands of parameters for which one finds similar chaotic behaviors in phase space.*
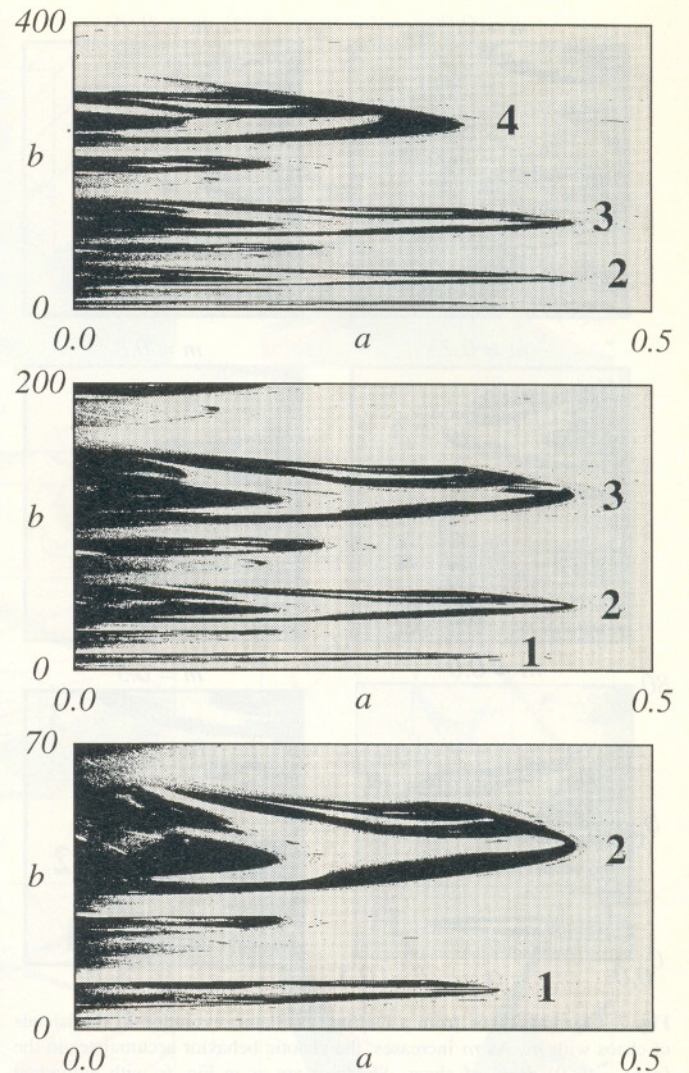

Fig. 6. Approximately self-similar islands of chaos (*in black*) embedded in a sea of regularity (*in white*), for the Duffing oscillator, (23), with $m = 0$ (i.e., standard trigonometric pumping). The numbers are simply labels to facilitate visual comparisons. Each individual figure displays 1200×600 Lyapunov exponents

What happens now with these islands of chaos if one applies a Jacobian pumping and varies m between the trigonometric and the hyperbolic limits?

Figure 7 shows the changes induced in the oscillator by the Jacobian excitation. One clearly sees that the net effect of varying m (i.e., the wave form and periodicity of the drive), is to *displace the islands of chaos in parameter space*. The effect of increasing m from $m = 0$ to about $m = 0.7$ is to push and compress all islands towards $(a, b) = (0, 0)$. Comparing the cases $m = 0.0$ and $m = 0.8$ one sees (i) the relative self-similarity between the islands labeled "2" and "3", and (ii) the compressions induced by the Jacobian excitation in both islands. As m increases towards the hyperbolic limit, more and more islands "come down", accumulating all of them in $(0, 0)$. In the limit $m \rightarrow 1$, all chaotic behavior collapses into the $(a, b) = (0, 0)$ drain. Therefore, by suitably choosing m one may "clean" wide parameter regions from chaotic behaviors. Further, since it is natural to expect the existence of a large variety of periodic motions in the pe-
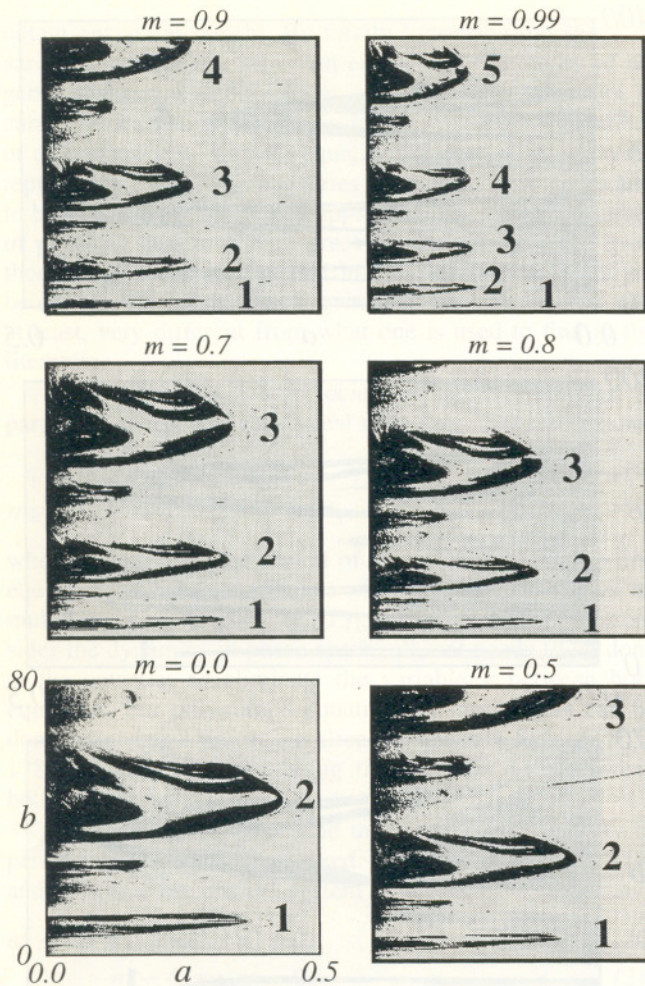
Fig. 7. Cleaning chaos from a Duffing oscillator: evolution of the islands of chaos with m. As m increases, the chaotic behavior accumulates in the $(a, b) = (0, 0)$ *drain* of chaos. *Shadings* are as in Fig. 6, with individual figures containing 600×600 exponents, except for $m = 0$ which shows 1200×1200 exponents. The numbers are simply labels to facilitate visual comparisons. The scales shown for $m = 0$ apply to all other pictures

riodic sea, one may well anticipate the possibility of using m to induce changes between motions of different periodicities without having to change a and/or b. The possibility of cleaning wide portions of the parameter space from chaos and the possibility of changing periodicity is of interest in experimental situations where external drives are easier to control than internal parameters [19].

The possibility of using external modulations to clean chaotic behaviors from dynamical systems is anticipated to have many interesting applications in modulated lasers as, for example, in CO_2 lasers either with modulation in the losses of the resonator, in the pump or in the resonator frequency, as considered, for example, in the works listed as [20]. Modulations are also of great interest for semiconductor lasers [21] and NMR lasers [22], to name just a few. We hope to report quantitative predictions for some of these systems soon.

5 Conclusions

This paper considered the parameter space of a ring cavity showing that it contains a great number of isoperiodic domains embedded in a sea of parameters for which the dynamics is characterized by aperiodic solutions (chaos). We described a simple model, (4), that contains the fundamental characteristics of the ring cavity but has the advantage of allowing one to obtain analytical insight from it. Using this advantage, it was possible to realize that the regularities in parameter space originate from a particularly beautiful set of numbers which satisfy certain "tunneling conditions" defined by (14) and (15). We demonstrated that the usual classification of trajectories in phase space is not necessary to understand the great number of regular features present in parameter space of dynamical systems defined by polynomial equations of motion. In particular, all superstable loci may be obtained directly from considerations based exclusively in parameter space, as exemplified by (22). Further, one may work directly in parameter space to derive the tunneling conditions and to use them, for example, to *predict* precisely parameter locations where one will find interesting phenomena such as the homoclinic phenomena that bothered Poincaré and many others since then.

We also considered the parameter space for a flow (i.e., a continuous-time dynamical system) in phase space, showing that for a driven Duffing equation there are islands of chaos embedded in a sea of regularity as the amplitude of the drive increases. By choosing the drive conveniently, one may displace the islands of chaos in parameter space, cleaning chaos from the system. The possibility of cleaning chaos is anticipated to be of interest for removing chaos from parameter space of, e.g., modulated lasers.

Knowing that the parameter space of the discrete-time model of the ring cavity contains so many self-similar shrimps of periodicity, it is natural to ask whether similar subdivisions might exist in the parameter space of continuous-time dynamical systems like the Duffing equation or a modulated laser. Thus, an interesting open question now is the detailed description of the "fine structure" of the sea of periodic motions in continuous-time dynamical system. We plan to address this question in subsequent work.

Appendix

Generating π from a non-periodic orbit

In this appendix, we show how to construct the number $\pi = 3.141592\ldots$ from the infinite sequence of numbers constituting a particularly interesting non-periodic orbit which is also a superstable orbit.

It is not difficult to show that for a specific value of the control parameter of the quadratic map, the building block of (4), one obtains the following general expression

$$\text{arccos } x_0 = \frac{\sqrt{1 - x_0^2}}{x_1 \, x_2 \, x_3 \, \ldots},$$

where the infinite sequence of numbers x_t is generated by the dynamical system

$$x_{t+1} = \sqrt{\frac{1}{2}(1 + x_t)}, \qquad t = 0, 1, 2, 3, \ldots .$$

As seen, for every initial condition $-1 \leq x_0 \leq 1$ *the equation above shows how every infinite sequence of points x_t conjures to produce a well-known trigonometric function.*

The particular number π is obtained by always choosing consistently the positive branch of the square-root function and starting iterations from the critical point $x_0 = 0$. Notice that the left-hand side of the formula above guarantees that there is no value of t in the future for which one will ever again be back to the starting point $x_0 = 0$, i.e., for all $t \neq 0$, one necessarily finds $x_t \neq 0$. The above choice $x_0 = 0$ generates a superstable orbit with infinite points, a chaotic sequence of points which conjure to produce a kind of order:

$$\pi = \frac{2}{x_1 \ x_2 \ x_3 \ \ldots} .$$

It is easy to verify numerically that this formula converges extremely fast to the known value of π. Many other numbers may be obtained in a similar way, for other choices of initial conditions.

Using the general formula above, one may obtain many other things, for example, an explicit formula relating the sequence of signs of each point x_t of the orbit to its precise location on the appropriate Riemann sheet. This is a simple consequence of the multivaluedness of the arccos function. The above results show that, by suitably combining the set of all initial conditions x_0 together with the set of all their descendents, one may generate a well-known periodic function and also generate a fundamental constant of mathematical physics.

References

1. K. Ikeda: Opt. Commun. **30**, 257(1979)
   K. Ikeda, H. Daido, O. Akimoto: Phys. Rev. Lett. **45**, 709 (1980)
   K. Ikeda, O. Akimoto: Appl. Phys. B **28** 170 (1982)
   K. Ikeda, K. Matsumoto: Physica D **29**, 222 (1987)
2. For a recent review of the field, see C.O. Weiss, R. Vilaseca: *Dynamics of Lasers* (VCH, Weinheim 1991)
3. J.A.C. Gallas: Phys. Rev. Lett. **70**, 2471 (1993)
4. D.W. McLaughlin, J.V. Moloney, A.C. Newell: Phys. Rev. Lett. **51**, 75 (1983)
5. S. Hammel, C.K.R.T. Jones, J.V. Moloney: J. Opt. Soc. Am. B **2**, 552 (1983)
6. W.J. Firth, E. Abraham, E.M. Wright, Appl. Phys. B **28**, 170 (1982)
   E. Abraham, W.J. Firth: Opt. Acta **30**, 1541 (1983)
   R.G. Harrison, W.J. Firth, C.A. Emshary, I.A. Al-Saidi: Phys. Rev. Lett. **51**, 562 (1983)
   W.J. Firth: In *Chaos*, ed. by A.V. Holden (Manchester Univ. Press, Manchester 1986) Chap. 7, pp. 135–157

7. J. Carr, J.C. Eilbeck: Phys. Lett. A **104**, 59 (1984)
8. H.E. Nusse, J.A. Yorke: *Dynamics: Numerical Explorations*, Springer Ser. Appl. Math. Sci., Vol.101 (Springer, Berlin, Heidelberg 1994)
9. J.A.C. Gallas, C. Grebogi, J.A. Yorke: Phys. Rev. Lett. **71**, 1359 (1993)
10. References may be obtained from any book on chaotic dynamics, for example, from the encyclopedic work of H.-O. Peitgen, H. Jürgens, D. Saupe: *Chaos and Fractals, New Frontiers of Science* (Springer, Berlin, Heidelberg 1992) and the many references therein
11. J.A.C. Gallas: Physica A **211**, 57 (1994); Physica A **202**, 196 (1994); Phys. Rev. E **48**, R4156 (1993)
12. Any linear term may be removed by a simple linear shift of the origin of x_t. Linear *and* cubic terms may be removed using appropriate Tschirnhausen transformations.
13. E. Schröder: Math. Ann. **2**, 317 (1870); Math. Ann. **3**, 296 (1871)
   B. Derrida, A. Gervois, Y. Pomeau: J. Phys. A **12**, 269 (1979)
   P. Collet, J.P. Eckmann: *Iterated Maps on the Interval as Dynamical Systems* (Birkhäuser, Basel 1980)
   S. Chang, M. Wortis, J.A. Wright: Phys. Rev. A **24** 2669 (1981)
   L. Glass, R. Perez: Phys. Rev. Lett. **48**, 1772 (1982)
14. J.A.C. Gallas: HLRZ Rep., KFA Jülich (preprint)
15. B.L. van der Waerden: *Algebra*, Vol. 1, 9th edn. (Springer, Berlin, Heidelberg 1993)
16. G. Duffing: *Erzwungene Schwingungen bei veränderlicher Eigenfrequenz und ihrer technische Bedeutung*, Samml. Vieweg **41/42** (Vieweg, Braunschweig 1918)
17. L.M. Milne-Thomson: In *Handbook of Mathematical Functions*, ed. by M. Abramowitz, I. Stegun (Dover, New York 1965) pp. 567, 582
18. G. Benettin, L. Galgani, J.M. Strelcyn: Phys. Rev. A **14**, 2338 (1976)
   G. Bennetin, L. Galgani, A. Giorgilli, J.M.Strelcyn: Meccanica **15**, 9 (1980); Meccanica **15**, 21 (1980)
   I. Shimada, T. Nagashima: Prog. Theor. Phys. **61**, 1605 (1979)
   M. Sano, Y. Sawada: Phys. Rev. Lett. **55**, 1082 (1985)
   A. Wolf, J.B. Swift, H.L. Swinney, J.A. Vastano, Physica D **16**, 285 (1985)
19. A.R. Zeni, J.A.C. Gallas: HLRZ Rep., KFA Jülich (preprint)
20. T. Yamada, R. Graham: Phys. Rev. Lett. **45**, 1322 (1980)
   H. Scholz, T. Yamada, H. Brand, R. Graham: Phys. Lett. A **82**, 321 (1981)
   F.T. Arecchi, R. Meucci, G. Puccioni, J. Tredicce: Phys. Rev. Lett. **49**, 1217 (1982)
   D.V. Ivanov, Ya.I. Khanin, I.I. Matorin, A.S. Pikovsky: Phys. Lett. A **89**, 229 (1982)
   J.R. Tredicce, N.B. Abraham G.P. Puccioni, F.T. Arecchi: Opt. Commun. **55** 131 (1985)
   T. Midavaine, D. Dangoisse, P. Glorieux: Phys. Rev. Lett. **55**, 1989 (1985)
   D. Dangoisse, P. Glorieux D. Hennequin: Phys. Rev. A **36**, 4775 (1987)
   T. Erneux, S.M. Baer, P. Mandel: Phys. Rev. A **35**, 1165 (1987)
   P. Glorieux: J. Phys. (Paris) **48**, C7, 433 (1987)
   P. Mandel, D. Dangoisse, T. Erneux: J. Opt. Soc. Am. B **5**, 1113 (1988)
21. C.H. Lee, T.H. Yoon, S.-Y. Shin: Appl. Phys. Lett. **46**, 95 (1985)
   Y.C. Chen, H.G. Winful, J.M. Liu: Appl. Phys. Lett. **47**, 208 (1985)
   Y. Hori, H. Serizawa, H. Sato: J. Opt. Soc. Am. B **5**, 1128 (1988)
22. E. Brun, B. Derighetti, D. Meier, R. Holzner, M. Ravani: J. Opt. Soc. Am. B **2**, 156 (1985)